

## NEW MID-INFRARED DIAGNOSTIC OF THE DUSTY TORUS MODEL FOR SEYFERT NUCLEI

TAKASHI MURAYAMA

Astronomical Institute, Graduate School of Science, Tohoku University, Aoba, Sendai 980-8578, Japan;  
murayama@astr.tohoku.ac.jp

HIDEAKI MOURI

Meteorological Research Institute, 1-1 Nagamine, Tsukuba 305-0052, Japan; hmouri@mri-jma.go.jp

YOSHIAKI TANIGUCHI

Astronomical Institute, Graduate School of Science, Tohoku University, Aoba, Sendai 980-8578, Japan;  
tani@astr.tohoku.ac.jp*Draft version July 30, 2018*

## ABSTRACT

We propose a new diagnostic of the “dusty torus” model for Seyfert nuclei. Dust grains in the torus are heated by the nuclear continuum, and reradiate mostly in the mid-infrared wavelengths. From the torus geometry, it is predicted that the emission at  $\lambda \leq 10 \mu\text{m}$  has strong dependence on the viewing angle. Since the dependence is predicted to be insignificant at  $\lambda \geq 10 \mu\text{m}$ , we study the flux ratio between  $3.5 \mu\text{m}$  (*L* band) and  $25 \mu\text{m}$ ;  $R(L, 25) = \log[(\nu_{3.5 \mu\text{m}} S_{\nu_{3.5 \mu\text{m}}}) / (\nu_{25 \mu\text{m}} S_{\nu_{25 \mu\text{m}}})]$ . In three different samples (optically selected, X-ray selected, and infrared selected samples) of Seyfert galaxies, the observed values of  $R(L, 25)$  between type 1 Seyferts (S1s) and type 2 Seyferts (S2s) are found to be clearly separated;  $R(L, 25) > -0.6$  for S1s while  $R(L, 25) < -0.6$  for S2s. This implies universality of their torus properties. With this result and the other observational characteristics, we investigate the most plausible torus model among those presented in Pier & Krolik (1992, 1993).

*Subject headings:* galaxies: Seyfert - infrared: galaxies

## 1. INTRODUCTION

Dusty tori around active galactic nuclei (AGNs) play an important role in the classification of Seyfert galaxies. (Antonucci & Miller 1985; see also Antonucci 1993 for a review). Seyfert galaxies observed from a face-on view of the torus are recognized as type 1 Seyferts (S1s) while those observed from a edge-on view are recognized as type 2 Seyferts (S2s). In this way, the dusty tori act as a material anisotropically obscuring the emission from their interior region.

Dusty tori themselves are also important emitting sources in AGNs. Dust grains within the torus absorb high-energy photons from the central engine, and re-emit them in the mid-infrared (MIR) regime. Therefore, infrared radiation from the dusty torus emission is useful in studying the physical properties of the tori in AGNs (e.g., Dopita et al. 1998 and references therein). Since the tori are quite optically thick, the MIR spectrum is predicted to have strong dependence on the viewing angle [Efstathiou & Rowan-Robinson 1990; Pier & Krolik 1992, 1993 (hereafter PK92 and PK93, respectively); Granato & Danese 1994; Granato, Danese, & Franceschini 1996, 1997]. When the torus is observed from a face-on view, its hot inner surface is seen and the emission at  $\lambda \leq 10 \mu\text{m}$  is enhanced. When observed from a edge-on view, the emission at  $\lambda \leq 10 \mu\text{m}$  is obscured and thus weakened. Heckman (1995) observed that the averaged ratio of *N*-band ( $10 \mu\text{m}$ ) flux to nonthermal radio flux is higher in S1s than in S2s (see also Giuricin, Mardirossian, & Mezzere 1995). Heckman, Chambers, & Postman (1992) observed a similar enhancement in radio-loud quasars (i.e., type 1) with respect to radio galaxies (i.e., type 2). PK93 observed that flux ratios of *L* band ( $3.5 \mu\text{m}$ ) to *N* band in S1s are higher than those in S2s. Fadda et al. (1998) observed that the MIR

spectrum is steeper (i.e., redder) in S2s than in S1s. However, further details of the MIR emission from dusty tori are unknown.

This paper proposes the flux ratio of *L* band to *IRAS*  $25 \mu\text{m}$  band as a new MIR diagnostic for the dusty torus model (§2). We compile the observational data from the literature (§3), compare the above ratios of S1s with those of S2s (§4), and discuss properties of the tori (§5).

## 2. NEW MIR DIAGNOSTIC

As stated above, the torus emission is expected to be more anisotropic at  $\lambda \leq 10 \mu\text{m}$  than at  $\lambda \geq 20 \mu\text{m}$  because the visibility of the inner wall of the torus is highly viewing angle dependent. Therefore, it is of interest to compare S1s with S2s in a flux ratio between  $\lambda \leq 10 \mu\text{m}$  and  $\lambda \geq 20 \mu\text{m}$ . Since the *IRAS* photometric data are available for most of the nearby Seyfert galaxies (Moshir et al. 1992), we adopt the flux ratio between *L* band and *IRAS*  $25 \mu\text{m}$  band,

$$R(L, 25) = \log[(\nu_{3.5 \mu\text{m}} S_{\nu_{3.5 \mu\text{m}}}) / (\nu_{25 \mu\text{m}} S_{\nu_{25 \mu\text{m}}})].$$

The basic concept of our new MIR diagnostic is schematically shown in Figure 1. Since the viewing angle dependence is more significant at  $3.5 \mu\text{m}$ , S2s are expected to have lower values of  $R(L, 25)$  than S1s.

Here we note that PK 93 used the flux ratio between *L* and *N* bands,  $R(L, N)$ , to compare S1s with S2s. However, the *N*-band flux is affected by a silicate line at  $9.7 \mu\text{m}$ . When the torus is observed from a edge-on view, the silicate line is seen as an absorption line, and thus both the fluxes in *L* and *N* bands are weakened. The difference between S1s and S2s in  $R(L, N)$  is thereby expected not to be as prominent as that in  $R(L, 25)$ .

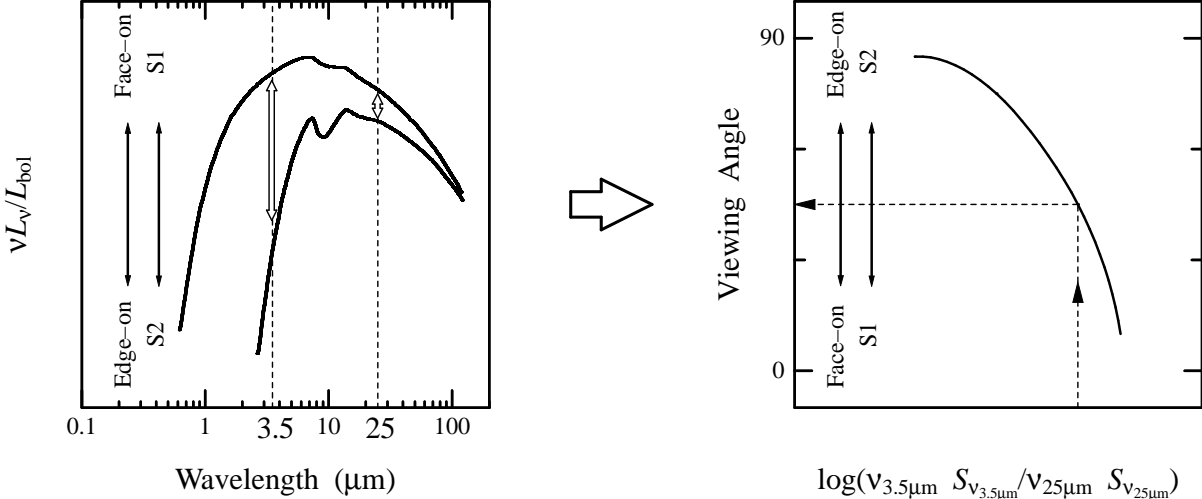


FIG. 1.— Basic concept of our MIR diagnostic. The left panel shows typical spectra of the torus emission for S1s (upper) and for S2s (lower). The right panel shows how the  $3.5\mu\text{m}$  to  $25\mu\text{m}$  flux ratio yields the viewing angle toward the torus.

### 3. DATA SAMPLE

To perform a statistical analysis with the MIR diagnostic defined in the previous section, we have compiled photometric data in  $L$ ,  $N$ , and *IRAS*  $25\mu\text{m}$  bands from the literature (e.g., Ward et al. 1987; Roche et al. 1991; Moshir et al. 1992; PK93). Since radiation from AGNs is anisotropic in most of the energy bands, it is difficult to construct a statistically complete sample. We instead adopt three samples chosen by different selection criteria. The first sample consists of the CfA Seyfert galaxies<sup>1</sup> (Huchra & Burg 1992), which provide a well defined collection of objects limited by the  $B$  magnitude of their host galaxies. The second sample is the one limited by the hard X-ray flux from 2 to  $10\text{ keV}$  (Ward et al. 1987). Since hard X-rays arise from the central engine itself and are not affected seriously by dust grains, this sample is expected to be fair at least for S1s. The third sample is taken from Roche et al. (1991). This sample is not complete but composed of  $N$ -band bright objects. For each object in this sample, Roche et al. (1991) observed an emission feature at  $11.3\mu\text{m}$ , which allows us to examine the presence or absence of any circumnuclear star formation activities. Our CfA, Ward, and Roche samples contain 18 S1s and 6 S2s, 20 S1s and 4 S2s, and 11 S1s and 11 S2s, respectively. Some objects are included in more than one sample. In total, there are 31 S1s and 14 S2s. Their basic data are summarized in Table 1.

Besides the dusty torus, several sources in Seyfert galaxies contribute to the observed MIR fluxes (see below). We exclude galaxies where the contamination with such sources appears to be significant. These galaxies are indicated in Table 1. The resultant final samples consist of 27 S1s and 5 S2s.

The *IRAS*  $25\mu\text{m}$  measurements were made with an aperture which is large enough to cover the entire galaxy ( $0.75' \times 4.6'$ ; Neugebauer et al. 1984). There could be contamination with the disk of the host galaxy. To find galaxies where the disk emission dominates over the torus emission, we use the compactness parameter  $CP$  at  $10\mu\text{m}$  (Devereux 1987),  $CP = f_{\text{cc}} \times S_{\nu_N} / S_{\nu_{12\mu\text{m}}}$ . Here  $S_{\nu_N}$  is the  $N$

band flux,  $S_{\nu_{12\mu\text{m}}}$  is the *IRAS*  $12\mu\text{m}$  flux, and  $f_{\text{cc}}$  is the color correction factor,  $f_{\text{cc}} = 0.12 S_{\nu_{12\mu\text{m}}} / S_{\nu_{25\mu\text{m}}} + 1.04$ . This compactness parameter gives an estimate on the ratio of the small-beam flux to the entire flux at  $10\mu\text{m}$ . The  $CP$  value of each galaxy is given in Table 1. Some objects exhibit  $CP > 1$ . This is due to uncertainties in the measurement or time variation of the nuclear flux. In such cases, we give  $CP = 1$ . The MIR fluxes of galaxies with  $CP < 0.5$  are likely to be dominated by the disk emission. These galaxies are not used in our following analysis.

On the other hand, the  $L$ - and  $N$ -band data given in Table 1 were obtained with small apertures ( $\phi \simeq 5'' - 10''$ ). In these data, the contamination with the host galaxy is unlikely to be important. From  $K$ -band images of Seyfert galaxies, Kotilainen et al. (1992) estimated the average light contribution from the host galaxy as 32 %. Zitelli et al. (1993) found that  $L$ -band images of Seyfert galaxies are more centrally concentrated than the  $K$ -band ones. Hence the contribution from the host galaxy to the  $L$ -band flux is less than  $\sim 30\%$ .

Seyfert galaxies often exhibit circumnuclear starburst activities, which could affect the MIR emission (see Keto et al. 1992 for the case of NGC 7469). Such objects are excluded from our analysis. As a signature of the starburst activity, we use emission features in the  $8 - 13\mu\text{m}$  regime (Roche et al. 1991). They are due to transient heating of polycyclic aromatic hydrocarbon molecules (PAHs) by UV photons from OB stars. Since PAHs are destroyed by X-rays, PAH features are absent in genuine AGNs (see Voit 1992 and references therein).

We also exclude narrow-line X-ray galaxies (NLXGs), i.e., S2s with strong hard X-ray emission (Shuder 1980; Véron et al. 1980; Ward et al. 1987). The central engine of these galaxies is believed to be hidden not by a dusty tori but by the disk of the host galaxy. Most of NLXGs are actually edge-on galaxies (see Ulvestad & Wilson 1984 and Keel 1980 for the cases of NGC 2992 and NGC 5506). Furthermore, Glass et al. (1981) reported that  $R(L, N)$  values of NLXGs are similar to those of S1s rather than those of S2s.

<sup>1</sup>The preliminary analysis based on the CfA Seyfert galaxies was reported in Murayama, Mouri, & Taniguchi (1997).

TABLE 1  
INFRARED PROPERTIES OF THE SAMPLE SEYFERT GALAXIES

Name <sup>a</sup>	<i>L</i> (Jy)	<i>N</i> (Jy)	<i>S</i> <sub>12 μm</sub> (Jy)	<i>S</i> <sub>25 μm</sub> (Jy)	<i>S</i> <sub>60 μm</sub> (Jy)	<i>S</i> <sub>100 μm</sub> (Jy)	<i>CP</i> <sup>b</sup>	<i>R</i> ( <i>L</i> , 25) <sup>c</sup>	Sample <sup>d</sup>	Reject <sup>e</sup>
Type 1 Seyfert										
2237+07	0.016	0.082	0.1400	0.3920	0.900	1.270	0.81	-0.54	C	
3A 0557-383	0.113	0.347	0.5289	0.6846	0.3223	< 0.5589	0.78	0.07	W R	
3C 120	0.090	0.220	0.2860	0.6350	1.283	2.786	1.00	0.00	W R	
Akn 120	0.0740	0.139	0.3191	0.4099	0.643	1.084	0.52	0.11	W	
ESO 141-G55	0.0640	0.184	0.2420	0.3522	0.5741	< 1.481	0.92	0.11	W	
I Zw 1	0.110	0.390	0.5118	1.211	2.243	2.643	1	-0.19	C R	
IC 4329A	0.227	0.760	1.082	2.213	2.030	1.661	0.90	-0.14	W R	
MCG -6-30-15	0.0877	0.286	0.3803	0.8088	1.087	1.096	0.97	-0.12	W	
MCG 8-11-11	0.075	0.296	0.6394	1.948	3.005	4.235	0.65	-0.57	W R	
Mrk 79	0.0543	0.200	0.3062	0.7625	1.503	2.363	0.87	-0.30	W	
Mrk 231	0.360	1.420	1.872	8.662	31.99	30.29	1	-0.53	C R	
Mrk 279*	0.032	0.076	0.1990	0.2890	1.200	1.970	0.46	-0.10	C	<i>CP</i> < 0.5
Mrk 335	0.123	0.210	0.3021	0.3777	0.3433	< 0.5673	0.83	0.37	C	
Mrk 509	0.113	0.220	0.3158	0.7018	1.364	1.521	0.91	0.06	W R	
Mrk 530	0.025	0.077	0.1800	0.1910	0.8560	2.140	0.50	-0.03	C	
Mrk 590	0.0469	0.169	0.1917	0.2214	0.4893	1.457	1	0.18	C W	
Mrk 766	0.0559	0.288	0.3855	1.295	4.026	4.658	1	-0.51	C	
Mrk 817	0.0619	0.357	0.3350	1.175	2.118	2.268	1	-0.42	C	
Mrk 841	0.0407	0.1445	0.1924	0.4726	0.4593	< 0.6176	1	-0.21	C W	
Mrk 1040	0.105	0.294	0.6104	1.315	2.555	4.551	0.63	-0.25	W	
NGC 3227	0.0783	0.263	0.6671	1.764	7.825	17.59	0.54	-0.50	C W	
NGC 3516	0.117	0.239	0.4258	0.8937	1.758	2.259	0.73	-0.03	C	
NGC 3783	0.131	0.400	0.8396	2.492	3.257	4.899	0.67	-0.43	W R	
NGC 4051*	0.077	0.297	0.8554	1.590	7.131	23.92	0.44	-0.46	C W R	<i>CP</i> < 0.5
NGC 4151	0.344	1.400	2.080	4.600	6.720	8.600	0.88	-0.27	C W R	
NGC 4593	0.081	0.182	0.3441	0.8089	3.052	5.947	0.70	-0.15	W	
NGC 5033*	0.0487	0.031	0.9452	1.148	13.80	43.85	0.04	-0.52	C	<i>CP</i> < 0.5
NGC 5273	0.016	0.134	0.1340	0.2420	0.9910	2.030	1	-0.33	C	
NGC 5548	0.0986	0.210	0.4006	0.7690	1.073	1.614	0.67	-0.04	C W	
NGC 7213	0.115	0.261	0.6063	0.7421	2.666	8.177	0.51	0.04	W	
NGC 7469*	0.1594	0.600	1.348	5.789	25.87	34.90	0.69	-0.71	C W R	PAH
Type 2 Seyfert										
Circinus*	0.701	6.00	19.58	71.29	248.7	315.9	0.45	-1.16	R	<i>CP</i> < 0.5
Mrk 266	0.007	0.306	0.2307	0.9765	7.432	11.07	1	-1.29	C	
Mrk 348	0.039	0.300	0.3080	0.8347	1.290	1.549	1	-0.48	R	
Mrk 533*	0.046	0.217	0.6724	1.896	5.588	8.146	0.44	-0.76	C R	<i>CP</i> < 0.5
NGC 1068	1.920	18.0	39.7	85.04	176.2	224.0	0.59	-0.79	C R	
NGC 1275	0.078	0.674	1.069	3.539	7.146	6.981	0.91	-0.81	R	
NGC 2110*	0.047	0.198	0.3488	0.8397	4.129	5.676	0.75	-0.40	R	NLXG
NGC 2992*	0.057	0.249	0.594	1.422	6.941	14.44	0.56	-0.55	W R	PAH, NLXG
NGC 3079*	0.073	0.091	1.523	2.272	44.5	89.2	0.07	-0.64	C	<i>CP</i> < 0.5
NGC 4388	0.074	0.404	0.9964	3.463	10.24	18.10	0.59	-0.82	C R	
NGC 5506*	0.313	0.643	1.282	3.638	8.409	8.886	0.69	-0.22	W R	NLXG
NGC 5929*	0.0073	0.0186	0.360	1.570	9.450	12.00	0.08	-1.48	C	<i>CP</i> < 0.5
NGC 7172*	0.132	0.141	0.4374	0.7612	5.712	12.29	0.40	0.09	W R	<i>CP</i> < 0.5, NLXG
NGC 7582*	0.201	0.877	1.620	6.436	49.10	72.92	0.82	-0.66	W R	PAH, NLXG

<sup>a</sup>Galaxies shown with asterisks are excluded from the analysis because of possible contamination to the infrared emission

<sup>b</sup>Compactness parameter defined in text

<sup>c</sup> $R(L, 25) = \log[(\nu_{3.5 \mu\text{m}} S_{\nu_{3.5 \mu\text{m}}}) / (\nu_{25 \mu\text{m}} S_{\nu_{25 \mu\text{m}}})]$

<sup>d</sup>C: the CfA sample; W: the Ward sample; R: the Roche sample

<sup>e</sup>Reasons for excluding from the analysis

#### 4. RESULTS

Figure 2 shows frequency distributions of  $R(L, 25)$  of S1s and S2s separately for the CfA sample (a), the Ward sample (b), the Roche sample (c), and the total sample (d). The galaxies excluded in the previous section are shown by white bars. Only the galaxies shown by black bars are used in the following analysis.

All of the S1s have  $R(L, 25) > -0.6$  while most of the S2s have  $R(L, 25) < -0.6$ . The S2 which lies exceptionally at  $R(L, 25) > -0.6$  is Mrk 348. This galaxy exhibits no silicate absorption feature at  $9.7 \mu\text{m}$  (Roche et al. 1991). Since the silicate absorption is a common property of S2s, Mrk 348 is considered to be in a face-on view like usual S1s. The absence of the broad-line region in this galaxy could result from, e.g., obscuration of the central region by a small cloud. There is no significant difference in the distributions of S1s and S2s among the three samples in Figures 2a–c, thus our samples is probably free of large orientation bias. If we apply the Kolmogorov-Smirnov (KS) test, the probability that the observed distributions of S1s and S2s originate in the same underlying population turns out to be 0.275 %. When galaxies shown by white bars are included, the distribution of S2s is different among the three samples. This difference is likely to come from the different sampling criteria.

Figure 3 compares the  $R(L, 25)$  ratio with the nuclear absolute  $B$  magnitude [ $M_B$  (nucleus)] for S1s. The  $M_B$  (nucleus) values are taken from Kotilainen, Ward, & Williger (1993) and Granato et al. (1993), and are used as a measure of the luminosity of the central engine. If the observed  $R(L, 25)$  ratio depends on the intrinsic luminosity of the central engine rather than the Seyfert type, there would be a certain relationship between  $R(L, 25)$  and  $M_B$  (nucleus). Since no clear correlation is seen in Figure 3, we conclude that the difference in the intrinsic nuclear luminosity does not affect the observed value of  $R(L, 25)$  in S1s. This conclusion is applicable to S2s because S1s and S2s are likely to have the same torus properties.

Finally, we show the frequency distributions of  $R(L, N)$  in Figure 4. The KS probability that the underlying populations of S1s and S2s are the same is 0.0404 %. Although this value is smaller than that for the  $R(L, 25)$  ratio, the separation between S1s and S2s in  $R(L, N)$  (Figure 4) is less clear than that in  $R(L, 25)$  (Figure 2). This is because the  $N$ -band emission is affected by the silicate feature at  $9.7 \mu\text{m}$ .

#### 5. DISCUSSION

The  $R(L, 25)$  values for the S1s are clearly separated from those for the S2s at the critical value of  $-0.6$ . This limits the extent to which the dusty torus can vary among Seyfert galaxies; such variations would add “noise” and cause overlap between the two types. Hereafter, we compare our results with theoretical torus models of PK92 and PK93, and investigate the model which agrees best with the observations.

Figure 5 shows the geometrical configuration assumed in PK92 and PK93. The torus surrounds cylindrically around the central engine and the broad-line region. The semi-opening angle  $\theta_{\text{open}}$  is given by the inner radius  $a$  and the height  $h$  of the torus;  $\theta_{\text{open}} = \tan^{-1}(2a/h)$ . The viewing angle  $i$  is defined as an angle between the rotation

axis of the torus and the line of sight. The critical viewing angle  $i_{\text{cr}}$  is defined such that the broad-line region is visible at  $i < i_{\text{cr}}$ . Since the actual torus should be clumpy and not have a sharp edge, we expect  $i_{\text{cr}} \geq \theta_{\text{open}}$ .

The torus emission is parameterized by the three quantities in the models of PK92 and PK93; 1)  $T$ : the effective temperature of the inner wall of the torus, 2)  $a/h$ : the inner aspect ratio, and 3)  $\tau_r$  and  $\tau_z$ : the radial and vertical Thomson optical depths. In the upper panel of Figure 6, we show the theoretical  $R(L, 25)$  values as a function of the viewing angle  $i$  for six dusty torus models of PK92 and PK93. In the lower panel, the observed  $R(L, 25)$  values are shown separately for S1s and S2s. For each of the models, the observed critical ratio,  $R(L, 25) = -0.6$ , yields a critical viewing angle. The results together with the model parameters are given in Table 2.

The derived critical viewing angle ranges from  $46^\circ$  to  $87^\circ$  (Models 1, 4, 5, and 6). Since Models 2 and 3 do not give the critical viewing angle, these models are not appropriate for dusty tori in Seyfert galaxies. To proceed further, we have to compare the results with other observational properties of Seyfert galaxies (see below).

Narrow-line regions of S2s often exhibit conical morphologies, which are due to shadowing of the nuclear ionizing continuum by the torus. The observed semi-opening angle of the cone  $\theta_{\text{open}}(\text{NLR})$  is thereby equal to the semi-opening angle of the torus  $\theta_{\text{open}}$ . Table 3 summarizes statistical results from observations of conical narrow-line regions (Pogge 1989; Wilson & Tsvetanov 1994; Schmitt & Kinney 1996). These results indicate  $\theta_{\text{open}}(\text{NLR}) \simeq 30^\circ$ . On the other hand, Model 1 has  $\theta_{\text{open}} = 11^\circ$ . Thus this model is not appropriate for dusty tori in Seyfert galaxies.

The critical viewing angle  $i$  can be estimated from the number statistics of S1s and S2s if we observe Seyfert nuclei from random orientations on the statistical ground,

$$\frac{N(\text{S1})}{N(\text{S1}) + N(\text{S2})} = 1 - \cos i_{\text{cr}} \text{ (stat)},$$

where  $N(\text{S1})$  and  $N(\text{S2})$  are the observed numbers of S1s and S2s, respectively (Miller & Goodrich 1990). Table 4 summarizes the results for three different surveys of Seyfert galaxies (Osterbrock & Shaw 1988; Salzer 1989; Huchra & Burg 1992). The derived critical viewing angles ranges from  $27^\circ$  to  $46^\circ$ . Since Models 4 and 5 give too large critical viewing angles ( $i_{\text{cr}} > 80^\circ$ ), they are not appropriate for dusty tori in Seyfert galaxies. Consequently, among the six models of PK92 and PK93, Model 6 with  $\theta_{\text{open}} = 31^\circ$  and  $i_{\text{cr}} = 46^\circ$  is the best torus model.

The  $R(L, 25)$  values of the S2s lie between  $-1.48$  and  $-0.6$ , which correspond to the viewing angles between  $86^\circ$  and  $46^\circ$ . On the other hand,  $R(L, 25)$  values of the S1s lie between  $-0.6$  and  $0.37$ . This range is not explained by Model 6. The locus of Model 6 in Figure 6 is drawn down only to  $i = 41^\circ$ . Since the  $R(L, 25)$  value at the smaller viewing angle is expected to be nearly constant, it would be impossible to reproduce the  $R(L, 25)$  ratio as high as  $0.37$ . One possibility that explains this higher ratio may be the  $3 \mu\text{m}$  bump often seen in type 1 AGNs. This bump may be attributed to thermal emission from hot dust grains with  $T \simeq 1300 \text{ K}$  (e.g., PK93). Because the models of PK92 and PK93 assumed that the host dust component is an additional source to the torus,  $R(L, 25)$

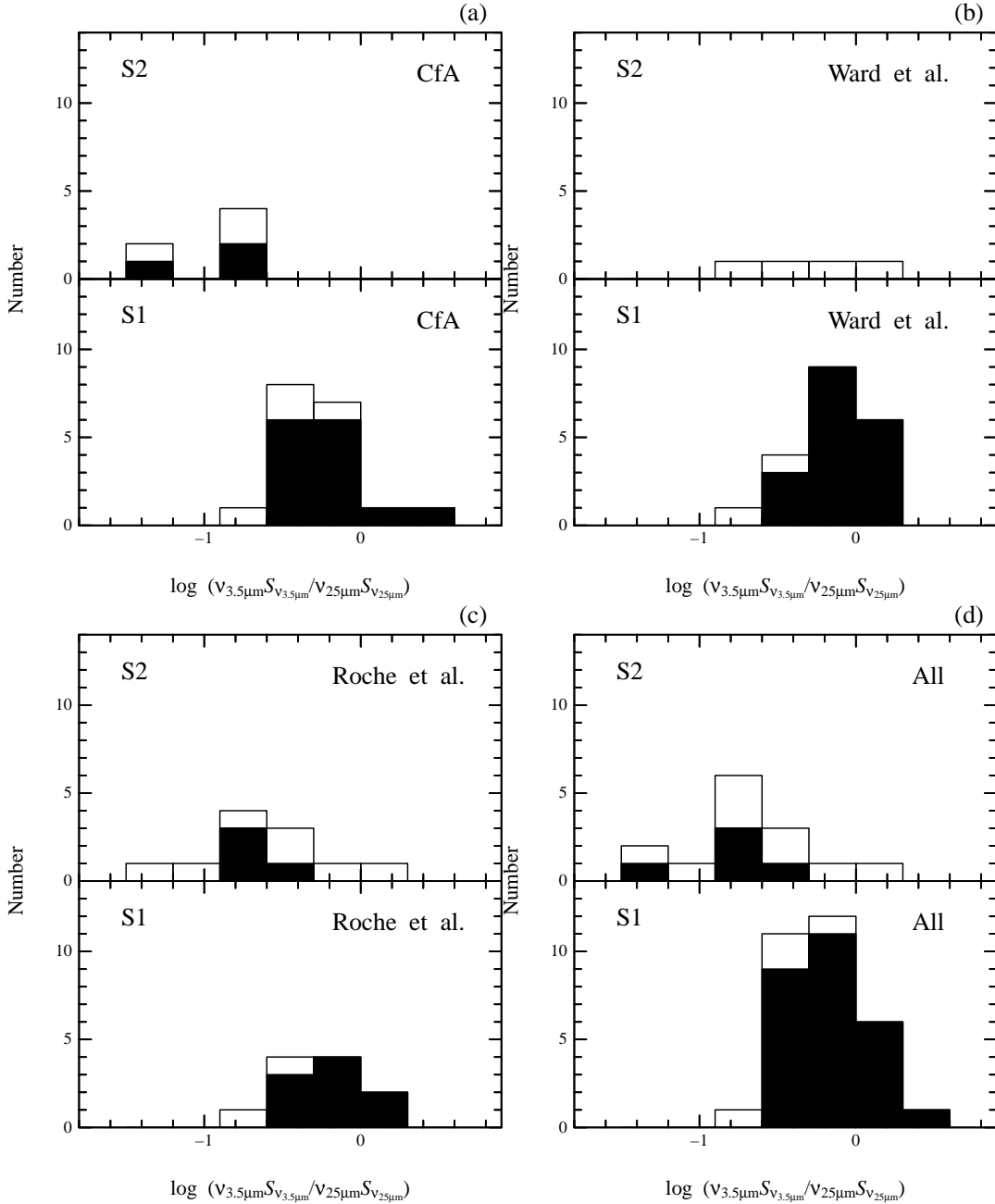


FIG. 2.— Histogram of  $R(L, 25)$  for the CfA Seyferts (a), the sample of Ward et al. (1987) (b), the sample of Roche et al. (1991) (c), and the total sample (d). Galaxies shown by white bars are likely to suffer from contamination and are not used in our analysis (see text and Table 1).

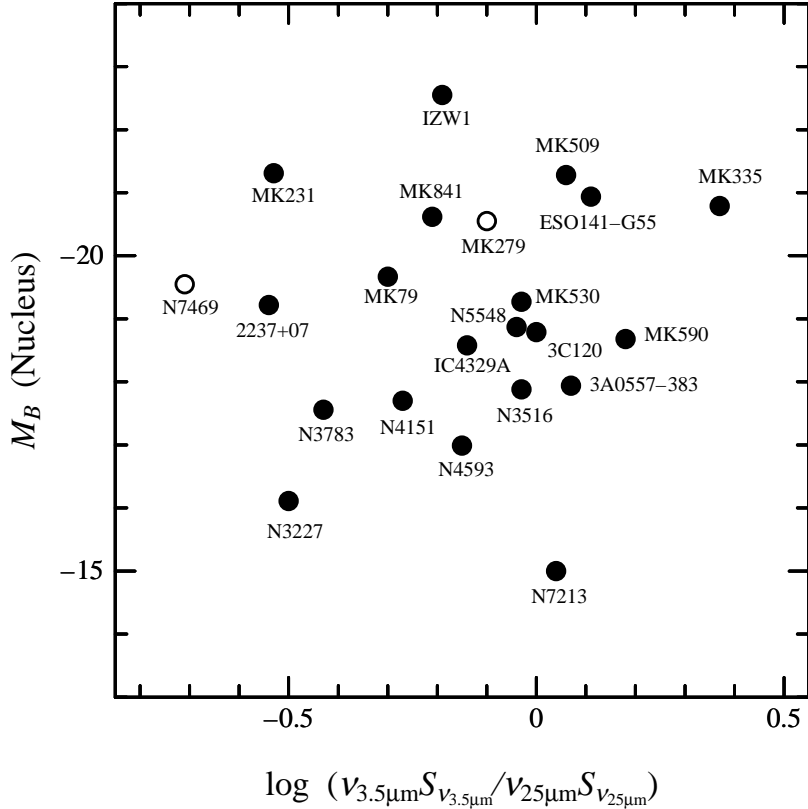


FIG. 3.— Diagram of  $R(L, 25)$  vs. absolute  $B$  magnitude of nuclei for S1s. Filled circles represent galaxies used in our analysis. Two open circles are Mrk 279 and NGC 7469, which are included in the sample but not used in our analysis (see text and Table 1). Nuclear  $B$  magnitudes were taken from Kotilainen, Ward, & Williger (1993) and Granato et al. (1993) which measured magnitudes of unresolved nuclear components deconvolved from two-dimensional CCD images of Seyfert galaxies. The Hubble constant of  $75 \text{ km s}^{-1} \text{ Mpc}^{-1}$  is assumed to obtain the absolute magnitudes.

TABLE 2  
THE DUSTY TORUS MODELS AND THE DERIVED CRITICAL VIEWING ANGLES

Model	$T^a$ (K)	$a/h^b$	$\tau_r^c$	$\tau_z^d$	$\theta_{\text{torus}}^e$ ( $^{\circ}$ )	$i_{\text{cr}}^f$ ( $^{\circ}$ )
1	1000	0.1	1	1	11	44
2	1000	0.3	0.1	0.1	31	...
3	1000	0.3	1	0.1	31	...
4	1000	0.3	1	1	31	87
5	800	0.3	1	1	31	82
6	500	0.3	1	1	31	46

<sup>a</sup>Effective temperature of the torus

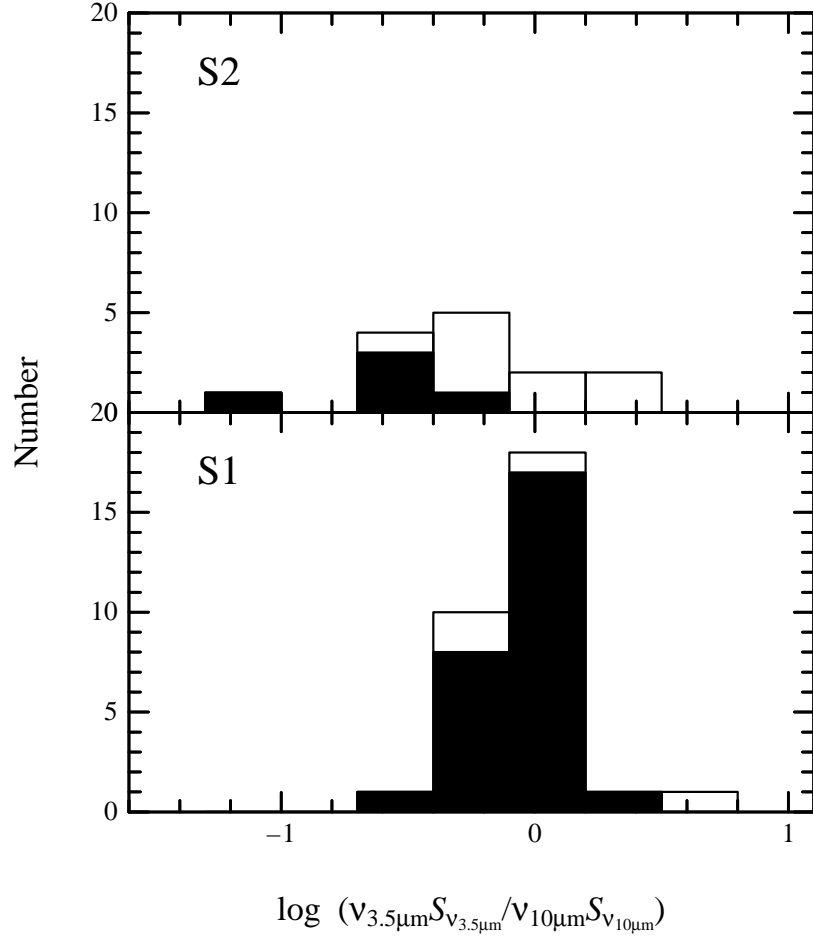
<sup>b</sup>Inner aspect ratio of the torus

<sup>c</sup>Radial Thomson optical depth of the torus

<sup>d</sup>Vertical Thomson optical depth of the torus

<sup>e</sup>Semi-opening angle derived from the inner aspect ratio

<sup>f</sup>Expected viewing angle of the torus



$$\log(v_{3.5\mu\text{m}}S_{3.5\mu\text{m}}/v_{10\mu\text{m}}S_{10\mu\text{m}})$$

FIG. 4.— Frequency distributions of  $R(L, N)$  for the total sample.

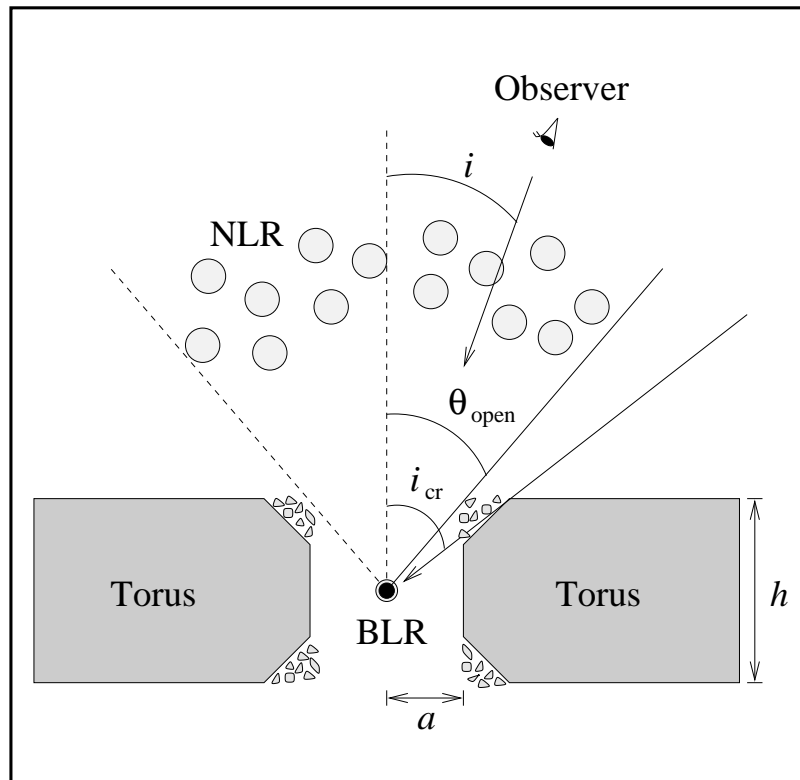


FIG. 5.— Schematic illustration of the geometrical configuration of the dusty torus model.

TABLE 3  
SEMI-OPENING ANGLES OF IONIZATION CONES OF SEYFERT NUCLEI

Reference	$N_{\text{Seyfert}}^{\text{a}}$	$\theta_{\text{open}}(\text{NLR})$
Pogge 1989	4	$26^{\circ} \pm 11^{\circ}$
Wilson and Tsvetanov 1994	11	$32^{\circ} \pm 8^{\circ}$
Schmitt and Kinney 1996	12	$29^{\circ} \pm 9^{\circ}$

<sup>a</sup>Number of the observed Seyfert galaxies

TABLE 4  
SEMI-OPENING ANGLES DERIVED FROM THE STATISTICS OF TYPE 1 AND TYPE2 SEYFERT GALAXIES

Reference	$N_{\text{S1}}^{\text{a}}$	$N_{\text{S2}}^{\text{b}}$	$f_{1/2}^{\text{c}}$	$i_{\text{cr}}(\text{stat})$
Osterbrock and Shaw 1988	6	9	0.125	$27^{\circ}$
Salzer 1989	9	7	0.20	$34^{\circ}$
Huchra and Burg 1992	25	23	0.435	$46^{\circ}$

<sup>a</sup>Number of type 1 Seyfert galaxies

<sup>b</sup>Number of type 2 Seyfert galaxies

<sup>c</sup>Number ratio between type 1 and type 2 Seyfert galaxies corrected for the completeness of the survey

is underpredicted at small inclination angles. Although it is controversial whether this host dust component is a separate component from the torus or the inner surface of the torus, those hot dust grains lie close to the central engine in either case. Since their emission is important only when the central region is clearly visible, the  $3 \mu\text{m}$  bump is negligible in S2s. Therefore the critical  $R(L, 25)$  and  $i_{\text{cr}}$  are not affected by the treatment of the  $3 \mu\text{m}$  bump.

We have examined only the small and sparse sets of the model parameters presented by PK92 and PK93. Further analyses with the larger and denser parameter sets are required to understand the torus properties in more detail. Nevertheless, our most important result, which has been obtained firstly with the new MIR diagnostic, is the clear separation in the  $R(L, 25)$  ratio between S1s and S2s. This strongly suggests that the torus properties do not vary among Seyfert galaxies. The effective temperature of the inner wall may be universal as a result of that the inner wall is formed by balancing the rate of dust destruction with the rate at which the torus clouds drift inward (Krolik & Begelman 1988; PK92). We suspect that there are also certain mechanisms confining the vertical structure of the torus and shaping the uniform semi-opening angle.

We thank K. Iwasawa and R. Antonucci for helpful comments and suggestions that improved the paper. TM is a JSPS Research Fellow. This work was financially supported in part by Grant-in-Aids for the Scientific Research (Nos. 07044054, 10044052, and 10304013) of the Japanese Ministry of Education, Science, Sports, and Culture.

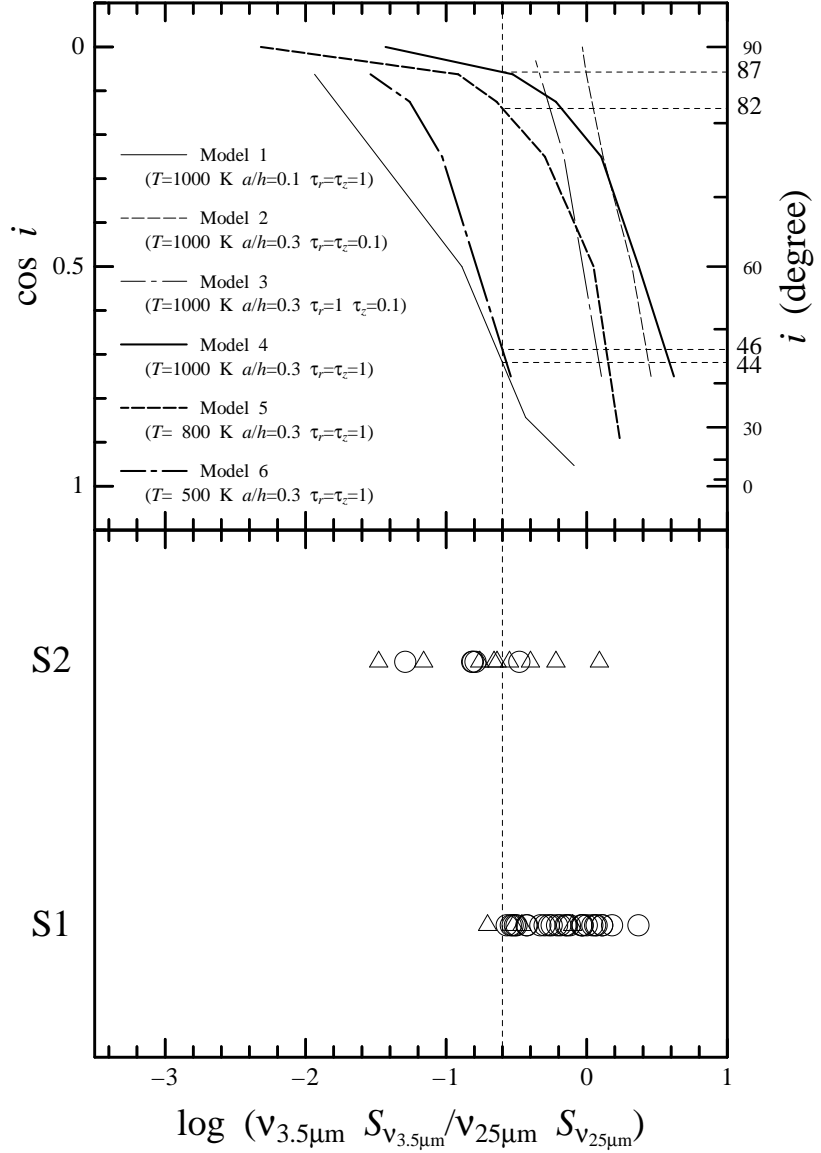


FIG. 6.— Upper panel: relationships between  $R(L, 25)$  and the viewing angle for six dusty torus models given in Table 4. Lower panel: distributions of the observed  $R(L, 25)$  values. Galaxies shown by open triangles are likely to suffer from contamination and are not used in our analysis (see text and Table 1).

## REFERENCES

Antonucci, R. 1993, *ARA&A*, 31, 473

Antonucci, R., & Miller, J. S. 1985, *ApJ*, 297, 621

Devereux, N. A. 1987, *ApJ*, 323, 91

Dopita, M. A., Heisler, C., Lumsden, S., Bailey, J. 1998, *ApJ*, 498, 570

Efstathiou, A., & Rowan-Robinson, M. 1990, *MNRAS*, 245, 275

Fadda, D., Giuricin, G., Granato, G. L., & Vecchies, D. 1998, *ApJ*, 496, 117

Giuricin, G., Mardirossian, F., & Mezzetti, M. 1995, *ApJ*, 446, 550

Glass, I. S., Moorwood, F. M., & Eichendorf W. 1982, *A&A*, 107, 276

Granato, G., & Danese, L. 1994, *MNRAS*, 268, 235

Granato, G., Danese, L., & Franceschini, A. 1996, *ApJ*, 460, L11

Granato, G., Danese, L., & Franceschini, A. 1997, *ApJ*, 486, 147

Granato, G., Zitelli, V., Bonoli, F., Danese, L., Bonoli, C., & Delpino, F. 1993, *ApJS*, 89, 35

Heckman, T. M. 1995, *ApJ*, 446, 101

Heckman, T. M., Chambers, K., & Postman, M. 1992, *ApJ*, 391, 39

Huchra, J., & Burg, R. 1992, *ApJ*, 393, 90

Keto, E., Ball, R., Arens, J., Jernigan, G., & Meixner, M. 1992, *ApJ*, 389, 223

Keel, W. C. 1980, *AJ*, 85, 198

Kotilainen, J. K., Ward, M. J., Boisson, C., Depoy, D. L., Smith, M. G., & Bryant, L. R. 1992, *MNRAS*, 256, 125

Kotilainen, J. K., Ward, M. J., Williger, G. M. 1993, *MNRAS*, 263, 655

Krolik, J. H., & Begelman, M. C. 1988, *ApJ*, 329, 702

Miller, J. S., & Goodrich, R. W. 1990, *ApJ*, 355, 456

Moshir, M. et al. 1992, Explanatory Supplement to the *IRAS* Faint Source Survey, Version 2, JPL-D-10015 8/92 (Pasadena: JPL)

Murayama, T., Mouri, H., & Taniguchi, Y. 1997, in Diffuse Infrared Radiation and the IRTS, edited by H. Okuda, T. Matsumoto, and T. L. Roellig, ASP Conf. Ser., Vol. 124, 381

Neugebauer, G. et al. 1984, *ApJ*, 278, L1

Osterbrock, D. E., & Shaw, R. 1988, *ApJ*, 327, 89

Pier, E., & Krolik, J. 1992, *ApJ*, 401, 99 (PK92)

Pier, E., & Krolik, J. 1993, *ApJ*, 418, 673 (PK93)

Pogge, R. W., 1989, *ApJ*, 345, 730

Roche, P. F., Aitken, D. K., & Smith, C. H. 1991, *MNRAS*, 252, 282

Salzer, J. 1989, *ApJ*, 347, 152

Schmitt, H. R., & Kinney, A. L. 1996, *ApJ*, 463, 498

Shuder, J. M. 1980, *ApJ*, 240, 32

Spinoglio, L., & Malkan, M. A. 1989, *ApJ*, 342, 83

Ulvestad, J. S., & Wilson, A. S. 1984, *ApJ*, 285, 439

Véron, P., Lindblad, P. O., uiderwijk, E. J., Véron, M. P., & Adam, G. 1980, *A&A*, 87, 245

Voit, G. M. 1992, *MNRAS*, 258, 841

Ward, M. J., Elvis, M., Fabbiano, G., Carleton, N. P., Willner, S. P., & Lawrence, A. 1987, *ApJ*, 315, 74

Wilson, A. S., & Tsvetanov, Z. I. 1994, *AJ*, 107, 1227

Zitelli, V., Granato, G. L., Mandolesi, N., Wade, R., & Danese, L. 1993, *ApJS*, 84, 185